The DOI for this manuscript is doi: 10.1175/JCLI-D-13-00615.1

The final published version of this manuscript will replace the preliminary version at the above DOI once it is available.

If you would like to cite this EOR in a separate work, please use the following full citation:

Simpkins, G., S. McGregor, A. Taschetto, L. Ciasto, and M. England, 2014: Tropical Connections to Climatic Change in the Extratropical Southern Hemisphere: The Role of Atlantic SST Trends. J. Climate. doi:10.1175/JCLI-D-13-00615.1, in press.

Tropical Connections to Climatic Change in the Extratropical Southern Hemisphere: The Role of Atlantic SST Trends.

Graham R. Simpkins, * Shayne McGregor, Andréa S. Taschetto

Climate Change Research Centre/ARC Centre of Excellence for Climate System Science, UNSW, Sydney, Australia

Laura M. Ciasto

Geophysical Institute, University of Bergen/Bjerknes Centre for Climate Research, Bergen, Norway

and Matthew H. England

Climate Change Research Centre/ARC Centre of Excellence for Climate System Science, UNSW, Sydney, Australia

Submitted to Journal of Climate

09/10/2013

Revisions Submitted

30/01/2013

* *Corresponding author address:* Graham R. Simpkins, Climate Change Research Centre, University of New South Wales, Sydney, NSW 2052.

E-mail: g.simpkins@unsw.edu.au

ABSTRACT

The austral spring relationships between sea surface temperature (SST) trends and the Southern Hemisphere (SH) extratropical atmospheric circulation are investigated using an atmospheric general circulation model (AGCM). A suite of simulations are analyzed wherein the AGCM is forced by underlying SST conditions in which recent trends are constrained to individual ocean basins (Pacific, Indian, Atlantic), allowing the impact of each region to be assessed in isolation. When forced with observed global SST, the model broadly replicates the spatial pattern of extratropical SH geopotential height trends seen in reanalyses. However, when forcing by each ocean basin separately, similar structures arise only when Atlantic SST trends are included. We further show that teleconnections from the Atlantic are associated with perturbations to the zonal Walker circulation and the corresponding intensification of the local Hadley cell, the impact of which results in the development of atmospheric Rossby waves. Thus, increased Rossby waves, forced by positive Atlantic SST trends, may have played a role in driving geopotential height trends in the SH extratropics. Furthermore, these atmospheric circulation changes promote warming throughout the Antarctic Peninsula and much of West Antarctica, with a pattern that closely matches recent observational records. This suggests that Atlantic SST trends, via a teleconnection to the SH extratropics, may have contributed to spring-time climatic change in the SH extratropics over the past three decades.

1. Introduction

The understanding of Antarctic climate change has often been hindered by the spatial and temporal paucity of observations. However, it is recently been recognized that surface air temperature (SAT) has increased across many parts of the Antarctic, particularly over the Antarctic Peninsula and continental West Antarctica, but with marked spatial and temporal variability (e.g. Turner et al. 2005; Marshall 2007; Monaghan et al. 2008; Steig et al. 2009; Schneider et al. 2012a; Bromwich et al. 2013, and references therein). Given the potential implications for ice sheet mass balance, and thereby global sea level rise (e.g. Rignot et al. 2011), an in-depth understanding of the nature and causes of long-term Antarctic SAT trends is required.

Antarctic SAT trends during austral summer (DJF) are dominated by rapid warming over the Antarctic Peninsula (e.g. Turner et al. 2005; Marshall 2007), and have been the focus of many investigations. This summer-time warming has largely been attributed to a trend toward the positive phase of the Southern Annular Mode (SAM), manifested as a pattern of negative (positive) pressure trends over the Antarctic continent (mid-latitudes), and consequently enhancing warm air advection over much of the Antarctic Peninsula (Thompson and Solomon 2002; Marshall et al. 2006; Marshall 2007; Thompson et al. 2011; Simpkins et al. 2012). This positive SAM trend has been linked to stratospheric ozone depletion, and to a lesser degree, increased greenhouse gases (Arblaster and Meehl 2006; Thompson et al. 2011; Simpkins and Karpechko 2012). While stratospheric ozone depletion peaks during spring, coupling with the SAM is restricted to the summer season when the stratosphere and troposphere are dynamically linked due to a decaying polar vortex (e.g. Thompson and Solomon 2002). Accordingly, SAM trends are also primarily constrained to the summer season, and as such, the SAM is unable to explain atmospheric circulation and temperature trends during other times (Thompson et al. 2011; Simpkins et al. 2012).

However, several recent studies have identified that SAT warming signals also extend throughout much of continental West Antarctica during both austral winter (JJA) and spring

(SON) (Steig et al. 2009; Schneider et al. 2012a). In fact, depending on the temperature reconstruction utilized, changes have been estimated to be ~0.5-1.0°C decade^{-1}, establishing West Antarctica as one of the fastest warming regions globally (Bromwich et al. 2013). These SAT trends have been increasingly linked to changes in low-latitude sea surface temperature (SST) and the corresponding impacts on the extratropical atmospheric circulation (Ding et al. 2011; Schneider et al. 2012a). For example, Ding et al. (2011) suggested that the wintertime increase in geopotential height over West Antarctica, and consequently the surface warming associated with warm air advection, may be part of stationary Rossby wave train forced by higher SSTs in the central Pacific. By contrast, spring-time atmospheric circulation trends are characterized by negative geopotential height anomalies over the high-latitude South Pacific, which similarly promotes warm air advection, and thereby positive SAT trends, over much of West Antarctica (Fig. 1a). A large proportion of these circulation trends have been connected to the modes of high-latitude atmospheric variability associated with the El Niño Southern Oscillation (ENSO), representing the Pacific South American (PSA) teleconnection patterns (Schneider et al. 2012a). Climatic change in West Antarctica is thus strongly sensitive to teleconnections associated with Pacific SST variability, as also identified in recent paleoclimate studies (Okumura et al. 2012; Steig et al. 2013).

Given such corroborating evidence that tropical SST trends may be driving, or contributing to, Antarctic SAT trends, it is prudent to establish a deeper understanding of tropical-extratropical interactions. On interannual time-scales, Southern Hemisphere (SH) teleconnections associated with SST variability in the Pacific have been well-documented (e.g. Karoly 1989; Mo and Higgins 1998; Garreaud and Battisti 1999; Ciasto and Thompson 2008; Ciasto and England 2011; Ding et al. 2011; Schneider et al. 2012a,b; Simpkins et al. 2012). In contrast, relatively few studies have examined the corresponding teleconnections arising from the Atlantic or Indian Oceans (exceptions including: Haarsma and Hazeleger 2007; Luffman et al. 2010; Timmermann et al. 2010; Taschetto et al. 2011; Okumura et al. 2012; Taschetto and Ambrizzi 2012; Li et al. 2014), particularly beyond interannual time-scales. Nevertheless, Luffman et al. (2010) suggest that long-term Indian Ocean warming likely has a minimal impact on the SH atmospheric circulation. Conversely, Okumura et al. (2012) identify links between Atlantic SST variability and the climate of West Antarctica, and argue that a change in the phase of this variability may have contributed to contemporary climate trends in this region, as also corroborated by Li et al. (2014). However, the dynamical mechanisms forcing this association remain largely unexplored, and as such, several questions remain.

Given the implications for SAT and broader-scale climatic change across Antarctica, this study aims to evaluate the extent to which atmospheric circulation trends in the SH extratropics may be forced by SST trends. Particular emphasis is placed on understanding teleconnections associated with the Atlantic, and thus we build upon the studies of Okumura et al. (2012) and Li et al. (2014). To this end, we use an atmospheric general circulation model (AGCM) in addition to observations to address the following: 1) What impact, if any, do SST trends in the Pacific, Indian, and Atlantic Oceans have on extratropical geopotential height trends in the SH between 1979-2009?, and 2) What are the physical mechanisms governing an atmospheric teleconnection between the Atlantic and the SH extratropics? Due to the spring-time peak apparent in both the amplitude of SAT trends (e.g. Schneider et al. 2012a; Bromwich et al. 2013), and the teleconnections emanating from the Pacific and Atlantic Oceans (e.g. Haarsma and Hazeleger 2007; Jin and Kirtman 2009; Schneider et al. 2012b; Simpkins et al. 2012), subsequent analyses are restricted solely to austral spring (September-November; SON).

The outline of the paper is as follows. Section 2 describes the observational records utilized in this study, and outlines the atmospheric model set-up and experimental design. Section 3 analyzes the patterns of atmospheric circulation associated with SST trends in individual ocean basins. The atmospheric dynamics of an Atlantic-Antarctic teleconnection are diagnosed in Section 4, and the cause of the Atlantic-related atmospheric circulation trend pattern examined in Section 5, along with climatic impacts of these trends. Finally, a summary and discussion are provided in Section 6.

2. Data and Numerical Experiments

a. *Observational and Reanalysis Datasets*

To both motivate and validate subsequent model simulations, a suite of observational and reanalysis datasets are used throughout this investigation. Monthly-mean sea surface temperature (SST) and sea ice concentration (SIC) are taken from the Hadley Centre Ice and Sea Surface Temperature (HadISST) dataset (Rayner et al. 2003). The data are available on a 1° x 1° latitude/longitude grid, and are derived using a blended analysis of in-situ measurements and satellite retrievals. We additionally use 18 of the most temporally continuous records of observed Antarctic surface air temperature (SAT) from the Reference Antarctic Data for Environmental Research (READER) archive (Turner et al. 2004), a collection of meteorological measurements obtained from Antarctic research and automatic weather stations. 500-hPa geopotential height (hereafter Z_{500}) and 950-hPa wind fields are taken from the ECMWF ERA-Interim analysis (Dee et al. 2011). Note that our results have also been repeated using alternative reanalysis products (e.g. NCEP-NCAR and NCEP2), and remain qualitatively similar to those presented here. Due to the sparse and temporally limited observational record, analyses are restricted to the post satellite era, 1979-2009, when data are more reliable, and spatial coverage is more complete over the SH mid-to-high latitudes (Bromwich and Fogt 2004). As described above, analyses are further constrained to austral spring (September-November; SON).

b. *Atmospheric Model Set-Up, Experimental Design, and Validation*

Various numerical experiments are performed using the National Center for Atmospheric Research (NCAR) Community Atmosphere Model, version 3 (CAM3), a complete description of which can be found in Collins et al. (2006) and Hurrell et al. (2006). CAM3 has been used extensively in investigations of climate research relevant to this study, including tropical climate variability (e.g. Deser et al. 2006), Antarctic climate variability and change (e.g. Bracegirdle et al. 2008; Raphael and Holland 2006), and tropical-extratropical interactions (e.g Okumura et al. 2012; Schneider et al. 2012a). For all simulations, CAM3 was configured at T42 horizontal resolution (approximately 2.8° latitude x 2.8° longitude), with 26 hybrid sigma-pressure vertical levels.

Prior to assessing the relationships between SST trends in individual basins and the extratropical atmospheric circulation, it is prudent to assess the capability of CAM3 to simulate the observed pattern of spring-time Z_{500} trends. To do so, CAM3 is forced with observed monthly-varying SST over the global oceans between January 1978 and December 2009 using the HadISST dataset; sea ice conditions are further prescribed as a repeating pattern of monthly-mean climatologies. This control experiment, termed SST_{GLO}, is integrated 12 times from different atmospheric initial conditions to account for the internal variability in the climate system. The ensemble mean is then assessed over austral spring during 1979-2009.

Figure 2 compares spring-time Z_{500} trends from ERA-Interim (shading) and the ensemble mean from the SST_{GLO} simulations (contours). It can be seen that the spatial pattern of modeled Z_{500} trends bears similarity to ERA-Interim, as illustrated by the gray hatching which marks where trends are consistent in sign. In particular, SST_{GLO} is successful in replicating the negative Z_{500} trends over the high-latitude South Pacific, congruous with the cyclonic wind pattern depicted in Figure 1a. Furthermore, the observed positive Z_{500} structure over the central mid-latitude Pacific is well-captured by SST_{GLO}. Nevertheless, Figure 2 also reveals discrepancies between simulated atmospheric circulation trends and their observational counterparts, largely in relation to latitudinal/longitudinal shifts in the location of Z_{500} structures. For example, relative to ERA-Interim, the modeled negative Z_{500} trends located over the South Pacific are shifted eastward towards the Amundsen Sea.

Additionally, SST_{GLO} fails to capture the observed positive Z_{500} trends centered over the South Atlantic and directly south of Australia. Finally, the magnitude of trends is typically underestimated in SST_{GLO}. However, the modeled Z_{500} trends are only associated with the applied SST forcing, and other factors may also contribute to the observed Z_{500} trend pattern depicted in Figure 2. Nonetheless, SST_{GLO} captures some notable aspects of the large-scale Z_{500} trends, making CAM3 a suitable tool to further investigate tropical-extratropical interactions over multi-decadal time-scales.

While the similarities evident in Figure 2 highlight that global SST trends likely play a role in forcing Z_{500} trends over the SH extratropics, this study aims to additionally separate and diagnose the impact of individual ocean basins. Thus further idealized model simulations are performed that isolate SST trends in the Pacific (SST_{PAC}), Indian (SST_{IND}), and Atlantic (SST_{ATL}) Oceans. For each of these experiments, CAM3 is forced with observed monthly-varying SST between January 1978 and December 2009 in the named basin (see Fig. 1b for spatial domains), but linearly detrended SST elsewhere. In SST_{PAC}, for example, observed SST are prescribed throughout the Pacific Ocean (i.e. including trends and variability), whereas detrended SST are prescribed in both the Indian and Atlantic Oceans (i.e. only including variability); thus, in this instance, modeled atmospheric circulation changes can be linked to Pacific SST trends. To minimize spurious atmospheric responses, linear damping was applied at the domain boundaries over a 10° latitude/longitude band. As in SST_{GLO}, the average of 12 ensemble members initialized from different atmospheric initial conditions are analyzed. Note that additional experiments performed using a repeating cycle of climatological SST beyond the basin of interest, rather than detrended SST as described above, produce quantitatively similar results to those presented here (not shown).

3. Modeled SH Atmospheric Response to SST Trends

Figure 3 displays spring-time Z_{500} trends from a) SST_{GLO}, b) SST_{PAC}, c) SST_{ATL}, and d) SST_{IND}; solid-red (dashed-blue) contours denote positive (negative) trends, and hatching highlights where 9 of 12 ensemble members agree on the sign of the trend, thus functioning as a measure of robustness across model integrations. Although geopotential height trends are presented only at 500-hPa, these are found to be largely consistent with trends evaluated at all levels of the troposphere (not shown), demonstrating an equivalent barotropic response over the mid-to-high southern latitudes. Significant differences in both the sign and structure of Z_{500} trends are seen across the SST experiments, particularly between SST_{PAC}/SST_{IND} and SST_{ATL}. For example, SST_{PAC} (Fig. 3b) is characterized by a robust positive pressure pattern extending over much of the South Pacific and into southern South America. This positive lobe is coupled with pronounced negative Z_{500} trends spanning across southern Australia and New Zealand. Similarly, SST_{IND} (Fig. 3d) is dominated by distinct positive trends centered over the Amundsen-Bellingshausen Seas, with less coherent structures observed elsewhere. Both SST_{PAC} and SST_{IND} thus simulate Z_{500} trends of opposite sign to SST_{GLO} over the high-latitude South Pacific (cf. Figs. 2, 3b, and 3d).

Interestingly, the South Pacific negative pressure center seen in SST_{GLO} and reanalyses is only reproduced when SST trends are applied in the Atlantic Ocean (Fig. 3c). In fact, the spatial pattern of Z_{500} trends associated with SST_{ATL} projects very strongly onto that of SST_{GLO}, such that large-scale consistency in trend structures, magnitudes, and sign are observed (cf. Figs. 3a and 3c). The spatial correlation between these two trend patterns is 0.76. However, subtle regional differences are also apparent when comparing SST_{ATL} to SST_{GLO}. For example, the negative Z_{500} trends located over the South Pacific are extended further northward into South America, and the positive Z_{500} trends cover a larger area extending over Australia and the sub-tropical Indian and Pacific Oceans. Nevertheless, the similarities between SST_{ATL} and SST_{GLO} suggests that SST trends in the Atlantic may play a significant role in forcing contemporary spring-time atmospheric circulation trends in the

SH extratropics.

Figure 3 thus demonstrates that the Z_{500} trend structures associated with SST_{GLO} more-closely reflect the impact of SST trends in the Atlantic, rather than the Pacific or Indian Oceans (cf. Figs. 3). Given that Pacific SST variability is known to strongly impact the extratropical atmosphere (e.g. Karoly 1989; Ciasto and Thompson 2008; Simpkins et al. 2012), it is somewhat surprising that SST_{PAC} does not display stronger similarities with SST_{GLO}. This may be related to the reduced amplitude of Pacific SST trends in comparison to the Atlantic (Fig. 1b), or to the lack of ocean-atmosphere coupling inherent in AGCM experiments. Furthermore, it is also important to note that SST_{ATL}, SST_{PAC} and SST_{IND} do not combine to reproduce the spatial pattern of Z_{500} trends modeled by SST_{GLO} (not shown). As illustrated by Figure 4, it is seen that the summed precipitation response for the individual basin experiments is considerably larger than that of SST_{GLO}, suggesting that non-linearities in convective precipitation, and the associated tropical-extratropical atmospheric dynamics, may play a role in driving the non-linear Z_{500} trends observed in Figure 3. Moreover, it must be remembered that complex inter-basin atmosphere-ocean interactions (e.g. Wang 2006; Keenlyside and Latif 2007; Kushnir et al. 2010; Timmermann et al. 2010; Ding et al. 2012; Luo et al. 2012; Santoso et al. 2012, and references therein) also complicate the diagnosis of tropical-extratropical interactions, particularly when isolating the impact of individual basins as in these idealized simulations. Regardless, the similarities between SST_{GLO} and SST_{ATL} in Figure 3 highlights that Atlantic SST trends may be a key factor influencing atmospheric circulation trends, motivating further investigation. As such, the next section determines the underlying atmospheric dynamics of the relatively little-explored Atlantic teleconnections to the SH extratropics.

4. Atlantic Teleconnections to the SH Extratropics: Atmospheric Dynamics

To diagnose the atmospheric dynamics governing Atlantic SST teleconnections to the SH extratropics, we perform daily-resolution perturbation experiments using CAM3, hereafter referred to as ATL_{PERT}. For these simulations, an SST anomaly is superimposed on the background climatological forcing across the tropical Atlantic Ocean, and the resulting atmospheric response is tracked through time. This SST perturbation, as illustrated in Figure 5, represents the spatial pattern of total spring-time SST trends linearly tapered between 30-40°N/S in the Atlantic, and chosen as previous studies highlight the importance of tropical latitudes in forcing extratropical responses (Okumura et al. 2012; Schneider et al. 2012a; Li et al. 2014). We perform 100 ATL_{PERT} simulations, wherein each member was initiated from different atmospheric conditions starting in September, and subsequently integrated for 60 days to give an end date in October/November. In each case, the Atlantic SST anomaly was held constant for the duration of simulation, while the global oceans followed a cycle of daily-interpolated climatological SST. Control simulations were performed as above, but without the superimposed SST anomaly. The approximate spring-time response to the anomalous Atlantic forcing was then determined by subtracting the individual control from the corresponding perturbation experiment, and analyzing the 100-member ensemble mean. In what follows, all figures illustrate the average response to the ATL_{PERT} over days 1-60 unless otherwise stated.

Figure 6 illustrates various tropical anomalies from the ATL_{PERT} experiments. In response to the applied SST forcing, upward vertical motion is initiated (Fig. 6a), generating anomalous convective precipitation across the equatorial Atlantic, but with maxima clearly discernible over the Caribbean Sea and off the coast of Guyana/Suriname/French Guiana (Fig. 6b, shading). By continuity, intensified surface westerlies are observed over ~0-120°W (Fig. 6b, vectors), driving an analogous pattern of surface convergence (not shown), which may be further enhanced by the introduced Atlantic/Pacific SST gradient. Corresponding upper level divergence structures are also apparent (Fig. 6a, vectors; Fig. 6c, shading), and as expected, project strongly onto the inter-related patterns of precipitation anomalies (cf. Figs. 6b-c, shading) given the relationship to latent heat release during deep convection. Consequently, poleward flowing divergent wind anomalies emerge in the upper troposphere (Fig. 6c, vectors). These are primarily constrained to ∼30-120°W, highlighting a regional response emanating from areas of strongest divergence, but representing a significant meridional perturbation to the large-scale circulation of the atmosphere.

Through mass balance, the Hadley Circulation also exhibits changes in association with the ATL_{PERT} experiments. Consistent with the regional divergent wind response (Fig. 6c), these Hadley Circulation modifications are also primarily regional, but represent a large enough disturbance to impact zonal-mean meridional streamfunctions (Fig. 7); note that calculations based on regional longitudes exhibit similar characteristics to those shown, but are typically stronger in magnitude. Climatologically (Fig. 7, contours), the general circulation is dominated by an anti-clockwise flowing SH Hadley Cell, in accord with the seasonal location of the Inter-Tropical Convergence Zone during austral spring. In response to the Atlantic thermal forcing, and the subsequent initiation of rising motion, surface convergence, and upper level divergence (i.e. the establishment of an anomalous zonal Walker circulation; Fig. 6), a pronounced intensification of the Hadley cell is observed (Fig. 7, shading); while a northward extension of the ascending branch is also apparent, the magnitude of the anomalies is an order less than the climatology so that the total expansion is modest. Changes to the other overturning cells are limited. It can thus be interpreted that the subsequent extratropical response is likely a consequence of perturbations to the Hadley Cell, which provides the mechanism by which tropical signals are transmitted to the extratropics. Specifically, the intensified overturning of the SH Hadley Cell enhances upper level convergence and subsidence at the descending branch (Fig. 6c); these features are again regional in character, and are most clearly expressed over the Eastern Pacific. This upper-level convergence, and the associated development of anomalous vorticity forcing, will have significant implications for the initiation of extratropical atmospheric Rossby waves.

Following Sardeshmukh and Hoskins (1988), the dynamics of Rossby waves can be diagnosed by analyzing the barotropic vorticity equation at 200-hPa. Specifically, the Rossby wave source (RWS), which quantifies vorticity forcing associated with low-level convergence and upper-level divergence, is calculated using:

$$RWS = -\overline{V_\chi \cdot \nabla(\zeta + f)} - \overline{(\zeta + f)D} \tag{1}$$

wherein V_χ and D are the divergent wind and divergence at 200-hPa, respectively, ζ is relative vorticity, and f the Coriolis parameter. The two terms in (1) represent the advection of vorticity by the divergent wind ($\overline{-V_\chi \cdot \nabla(\zeta + f)}$), and vorticity generation associated with vortex stretching ($\overline{(\zeta + f)D}$). Figure 8 displays the time-averaged RWS associated with the ATL_{PERT} experiments, and reveals a complex structure of anomalies primarily restricted to the eastern Pacific and Atlantic basins. Analysis of the vorticity budget indicates that the total RWS is predominantly governed by vortex stretching. As such, these two patterns project strongly onto one another, and thereby the corresponding pattern of 200-hPa divergence (cf. Figs. 6c, 8a-b). Nevertheless, although second order, the final solution is also modified by the vorticity advection term (Fig. 8c).

In response to the substantial upper level divergence (Fig. 6c), several pronounced RWS features are apparent over the Caribbean Sea despite the relatively weak planetary vorticity. Nonetheless, background climatological conditions will likely inhibit Rossby wave development from these locations due to the lack of an associated wave guide (Hoskins and Ambrizzi 1993; Lee et al. 2009). Of considerable note to this study, however, is the distinct negative RWS region that emerges at the convergent boundary of the intensified Hadley Cell in the East Pacific (∼70-130°W, ∼20-40°S). In this instance, it is these extratropical sources, driven remotely through changes in the local Hadley Circulation, that initiate the development of Rossby waves.

Here, Rossby wave evolution is examined by tracking Z_{500} anomalies averaged over days a) 1-3, b) 4-6, and c) 7-12 (Fig. 9); note the contrasting color axes. In response to the thermal forcing, negative pressure anomalies initially develop over the tropical Atlantic Ocean (Fig. 9a), forcing an anomalous zonal Walker circulation (Fig. 6a). By days 3-5, however, these tropically-sourced signals have been transferred to the extratropics via subsequent changes to the local Hadley Circulation (Fig. 7), matching the time-scales noted by Tyrrell et al. (1996). The resultant vorticity forcing, and thus RWS (Fig. 8), subsequently initiates a Rossby wave, as clearly expressed as a pattern of positive and negative Z_{500} anomalies located east of South America and south of Africa, respectively (Fig. 9b). Over time, these Z_{500} anomalies strengthen in magnitude and begin to propagate eastward with the climatological flow of the subtropical jet (Fig. 9c), allowing extratropical anomalies to be transferred circumglobally. These eastward propagating features are further identifiable in a time-longitude Hovmöller analysis of Z_{500} anomalies averaged over 30-60°S (Fig. 10). In particular, negative Z_{500} anomalies are simulated over the high latitude South Pacific (i.e. in the vicinity of the Amundsen-Bellingshausen Seas), with implications for the climate of West Antarctica.

A dynamical link has therefore been identified between perturbations in tropical Atlantic SST and atmospheric circulation changes in the SH extratropics, as summarized schematically in Figure 11. Specifically, thermal forcing in the tropical Atlantic drives changes to the zonal Walker circulation, whereby the corresponding anomalous vertical velocities and upper level divergence subsequently produce an intensification of the local Hadley circulation. In doing so, upper level convergence is enhanced at the descending branch of the Hadley Cell, which consequently becomes a source of Rossby waves that propagate with the climatological mean flow. Consistent with previous studies, we therefore find that the local Hadley circulation, which itself is perturbed through an anomalous zonal Walker circulation, provides the key dynamical connection between the tropics and extratropics, allowing for the development of Rossby waves well-removed from the tropical source of disturbance (Sardeshmukh and Hoskins 1988; Dréevillon et al. 2003; Hoskins and Ambrizzi 1993; Rasmusson and Mo 1993; Tyrrell et al. 1996).

5. The Connection between Atlantic SST and Climatic Change in the SH Extratropics

While the physical processes connecting tropical Atlantic SST variability to the extratropical atmospheric circulation have been established (e.g. as summarized in Fig. 11), it remains to be seen how these dynamics relate to the Z_{500} trend structure simulated by SST_{ATL} (Fig. 3c), and by deduction, how Atlantic SST trends may have influenced the observed pattern of circulation change over the past 3 decades. Here, we therefore synthesize the dynamical information gained from Section 4 and place it in the context of the SST_{ATL} experiments.

To establish the approximate spring-time Z_{500} structures associated with propagating Rossby waves (Fig. 10), Z_{500} anomalies from the ATL_{PERT} experiments are averaged over days 1-60. Figure 12 compares the resulting time-mean anomalies (shading) with the corresponding Z_{500} trends simulated by SST_{ATL} (contours; as in Fig. 3c). Despite the contrasting experimental design, Figure 12 illustrates that the two Z_{500} patterns possess many similarities. For example, both display negative Z_{500} anomalies in the vicinity of the South Pacific, along with positive anomalies spanning the Indian and east Pacific Oceans. Several shifts in the location of Z_{500} structures are also apparent, as evidenced by the more-southerly extension of positive ATL_{PERT} Z_{500} anomalies over the South Atlantic compared to the trends. These differences may simply be attributed to the contrasting boundary conditions used for the two experiments, i.e. constant tropical SST forcing in ATL_{PERT}, in contrast to time-varying SST forcing over all Atlantic latitudes/longitudes in SST_{ATL}. Nevertheless, spatial correlations between the two Z_{500} structures are 0.50. As such, it can be suggested that the Z_{500} trend pattern associated with SST_{ATL} may emerge in relation to the time-averaged impact of propagating Rossby waves over the spring season.

To determine whether the SST_{ATL} Z_{500} trends result from enhanced Rossby wave activity, trends are calculated for each of the components responsible for their initiation (i.e. each stage of Fig. 11). Figure 13 illustrates the spring-time trends for a) vertical velocity (shading) and U/W wind (vectors) averaged over 5°N - 5°S, b) convective precipitation (shading) and 950-hPa wind (vectors), c) 200-hPa divergence (shading) and divergent wind (vectors), and d) Rossby wave source at 200-hPa from the SST_{ATL} experiments. In each case it is seen that the pattern of trends projects strongly onto the corresponding anomalies associated with the ATL_{PERT} experiments (cf. Figs. 6, 8, 13), highlighting that similar atmospheric dynamics likely force both Z_{500} patterns.

In particular, Atlantic warming causes marked changes to the equatorial zonal circulation, manifested as trends towards enhanced upward vertical velocities (Fig. 13a), increased precipitation (Fig. 13b, shading), surface convergence (not shown), and thus upper level divergence (Fig. 13c, shading), over Central America and the tropical Atlantic. Accordingly, strengthened poleward flowing divergent winds emerge over the East Pacific/South American continent (Fig. 13c, vectors), which in turn, intensify the local Hadley circulation (not shown), enhance upper-level convergence at the descending branch (Fig. 13c, shading), and magnify RWS activity at this location (Fig. 13d). The right-hand panels of Figure 13 illustrate the equivalent trends for the SST_{GLO} experiments, and correspond strongly to those of SST_{ATL}. This similarity suggests that enhanced Atlantic SST (Fig. 1b), and the resulting impact of heightened Rossby wave activity, likely drives the simulated atmospheric circulation changes seen in both SST_{ATL} and SST_{GLO}, and thus explains their resemblance in Z_{500} structures (cf. Figs. 3a and 3c). Furthermore, the similarity between SST_{GLO} and reanalyses (Fig. 2) indicates that observed Z_{500} trends are likely to be heavily influenced by teleconnections emanating from the tropical Atlantic. By contrast, SST_{PAC} and SST_{IND}

display conflicting patterns (not shown), demonstrating that they likely play a lesser role in forcing the global response; for example, the spatial correlation between SST_{GLO} precipitation trends and SST_{PAC} is 0.26, compared to 0.15 for SST_{IND}, and 0.70 for SST_{ATL}.

Given the established impacts on the atmospheric circulation, Atlantic-related teleconnections also have broader-scale climatic implications, driven largely by thermal advection associated with the corresponding wind changes (e.g. Ding et al. 2011; Okumura et al. 2012; Schneider et al. 2012a; Li et al. 2014). Figure 14 displays spring-time SAT (shading) and surface wind (vectors) trends from the SST_{ATL} experiments, and observed SAT trends from Antarctic research stations (colored dots); note that the spatial structure of SST_{ATL}-related trends is similar at all levels of the troposphere, demonstrating an equivalent barotropic response (not shown). In association with the negative Z_{500} trends simulated over the high-latitude South Pacific (Fig. 3c), a pattern of cyclonic wind trends are established over this region (Fig. 14, vectors). As a result, anomalous onshore (northerly) winds drive warm air advection, and thus positive temperature trends, over the Antarctic Peninsula and eastern West Antarctic (Fig. 14, shading), coincident with the observed pattern of SAT trends (Fig. 14, colored dots). Whilst the magnitude of modeled temperature trends is approximately half those of observations, it must be remembered that complex feedback mechanisms, unresolved by an AGCM, may accentuate the magnitude of observed temperature trends. Conversely, offshore (southerly) winds enhance cold air advection over the Ross and Amundsen Sea regions, driving negative temperature trends that are largely absent from SAT reconstructions (e.g. Schneider et al. 2012a). However, this cooling trend is consistent with the observed pattern of sea ice expansion evident in the Ross Sea (Fig. 1a, shading) (e.g. Parkinson and Cavalieri 2012; Stammerjohn et al. 2012; Simpkins et al. 2013). Through driving changes in atmospheric circulation, teleconnections emanating from the tropical Atlantic may therefore play a prominent role in forcing climatic change in Antarctica, particularly in relation to the positive spring-time temperature trends observed in the Antarctica Peninsula.

6. Summary and Discussion

Several recent studies have identified a link between trends in tropical SST and large-scale circulation changes over the SH extratropics, prompting further investigation into tropical-extratropical interactions beyond interannual time-scales. Here, we use a suite of idealized numerical experiments performed with the CAM3 AGCM to document the spring-time relationships between SST trends in the Pacific, Indian, and Atlantic Oceans and the SH extratropical atmospheric circulation. Particular emphasis was given to diagnosing the impact of the Atlantic Ocean, a teleconnection which has received little attention in the literature to-date. The key conclusions from this study include:

1) *SST trends have likely played a role in forcing spring-time atmospheric circulation trends in the SH extratropics.*

Forcing CAM3 with observed SST over 1979-2009 (SST_{GLO}) captures several notable features of Z_{500} trends seen in reanalyses (Fig. 2), suggesting that such structures may be driven, at least partially, by global SST trends. Separating the SST influence of the Pacific, Indian and Atlantic basins reveals differences in the associated atmospheric teleconnection patterns, particularly in regard to the sign of changes over the high-latitude South Pacific (Fig. 3). Both Pacific (SST_{PAC}) and Indian (SST_{IND}) experiments, for example, invoke a positive Z_{500} trend in this location, promoting a contrasting pattern of circulation trends to those seen in the reanalyses. It is only when SST trends in the Atlantic Ocean are included (SST_{ATL}) that a negative Z_{500} trend is simulated over the South Pacific, bearing a marked similarity to the structures associated with SST_{GLO}. As such, Atlantic SST trends are suggested to have influenced the observed atmospheric circulation trends in the SH extratropics.

2) *Atlantic teleconnections to the SH extratropics are driven via changes to the zonal tropical circulation, corresponding perturbations to the local Hadley cell, and the subsequent initiation of atmospheric Rossby waves.*

Further AGCM experiments (ATL_{PERT}) were used to diagnose the atmospheric dynamics controlling Atlantic-Antarctic teleconnections. As summarized schematically in Figure 11, increased tropical Atlantic SST establishes marked changes to the zonal Walker circulation, expressed as anomalous upward motion (Fig. 6a), enhanced precipitation (Fig. 6b), and upper level divergence (Fig. 6c) across the tropical Atlantic, changes which may be further enhanced by the introduction of an SST gradient between the Pacific and Atlantic. By continuity, the upper-level divergent winds induce anomalous poleward flow (Fig. 6c), which intensifies the local Hadley circulation (Fig. 7), and enhances convergence at the descending branch (Fig. 6c). This, in turn, favors the initiation of Rossby waves at the convergent boundary (Fig. 8), which subsequently propagate and strengthen in time (Figs. 9 and 10) with implications for the Antarctic climate. Thus, consistent with previous studies (e.g. Dréevillon et al. 2003; Rasmusson and Mo 1993; Tyrrell et al. 1996), the Hadley circulation (itself modified through an anomalous zonal circulation) provides a direct link between the tropics and extratropics, and consequently, a mechanism by which Rossby waves can be established far from the tropical heat source in the Atlantic.

3) *Enhanced Rossby wave activity forced by Atlantic SST trends may have influenced climatic change in the SH extratropics.*

Spring-time Z_{500} trends simulated by SST_{ATL} represent the time-averaged impact of increased and/or strengthened Rossby waves (Figs. 12 and 13) associated with higher SST in the Atlantic Ocean (Fig. 1b). The similarities between the Z_{500} structures of SST_{ATL}, SST_{GLO} and reanalyses (Figs. 2 and 3) therefore suggests that observed Z_{500} trends may also be related, at least in part, to Atlantic SST trends. Owing to changes in regional atmospheric circulation, Atlantic teleconnections also greatly impact the Antarctic climate. In particular, the cyclonic wind trends simulated over the high-latitude South Pacific promote warm air advection over the Antarctic Peninsula, driving a pattern of positive temperature trends similar to observations (Fig. 14). Teleconnections associated with Atlantic SST variability may thus represent a significant mechanism driving climatic change in the SH extratropics.

These results add to the growing body of evidence which suggests that tropical trends are key factors forcing climatic change over the SH high-latitudes (e.g. Ding et al. 2011; Okumura et al. 2012; Schneider et al. 2012a; Li et al. 2014). In particular, we emphasize the importance of (the little-explored) Atlantic teleconnections in driving spring-time Z_{500}, and thereby SAT, trends over the South Pacific and West Antarctic, building upon similar conclusions made by Okumura et al. (2012) and Li et al. (2014). In doing so, these results contrast with previous studies that largely attribute spring-time trends to the Pacific. Schneider et al. (2012a), for instance, relate geopotential height trends to higher SSTs in the tropical/sub-tropical Pacific Ocean, and a resulting increase in the Rossby wave train associated with the PSA teleconnection patterns. However, our model simulations produce Z_{500} trends of opposite sign to observations when forced with Pacific SST variability (SST_{PAC}; Fig. 3b). While contrasting methodologies make it difficult to discern the cause of such differences, it is clear that further work is needed to clarify the relationships between trends in tropical SST and extratropical Z_{500}; for example, the relative role of the Atlantic and Pacific remains uncertain, as do the impacts of inter-basin interactions and the function of atmosphere-ocean coupling. Moreover, while simulations performed using CAM4 reproduce the main findings of this investigation (see Li et al. 2014), future work is needed to validate the robustness of these results across independent AGCMs, particularly given that the climatic impacts of Atlantic SST variability can be highly model dependent (e.g. Hodson et al. 2010).

Regardless, this study demonstrates that Atlantic SST trends need to be considered when diagnosing the mechanisms forcing climatic change in the SH extratropics. As such, understanding multi-decadal SST variability (linked namely to the Atlantic Multi-decadal Oscillation (AMO; Deser et al. 2010)), and future projections of Atlantic SST under increased greenhouse gas concentrations, could offer improved scope for prediction of longer-term trends in Antarctica. Nevertheless, it is important to note that other factors will continue to affect the SH extratropical climate in conjunction with the SST-forced changes described here. For example, both coupled atmosphere-ocean-sea ice feedbacks (unresolved in these AGCM experiments) and natural variability may have contributed to the observed trends over 1979-2009, and will likely continue to do so under an evolving climate.

Acknowledgments.

The authors thank the three anonymous reviewers for their helpful and valuable comments. GRS was supported by a University of New South Wales University International Postgraduate Award. LMC was supported by the Research Council of Norway through the Earthclim (207711/E10) project. This work was also supported the Australian Research Council, including the ARC Centre of Excellence for Climate System Science. Computer time was awarded under the Merit Allocation Scheme on the NCI National Facility at the ANU. The use of the NCAR CAM3 model is gratefully acknowledged, along with the institutions responsible for providing the observational and reanalysis datasets.

REFERENCES

Arblaster, J. M. and G. A. Meehl, 2006: Contributions of External Forcings to Southern Annular Mode Trends. *J. Clim.*, **19**, 2896–2905, doi:10.1175/JCLI3774.1.

Bracegirdle, T. J., W. M. Connolley, and J. Turner, 2008: Antarctic climate change over the twenty first century. *J. Geophys. Res.*, **113**, 3103, doi:10.1029/2007JD008933.

Bromwich, D. H. and R. L. Fogt, 2004: Strong Trends in the Skill of the ERA-40 and NCEP NCAR Reanalyses in the High and Midlatitudes of the Southern Hemisphere, 1958 2001(. *J. Clim.*, **17**, 4603–4619, doi:10.1175/3241.1.

Bromwich, D. H., J. P. Nicolas, A. J. Monaghan, M. A. Lazzara, L. M. Keller, G. A. Weidner, and A. B. Wilson, 2013: Central West Antarctica among the most rapidly warming regions on Earth. *Nature Geoscience*, **6**, 139–145, doi:10.1038/ngeo1671.

Ciasto, L. M. and M. H. England, 2011: Observed ENSO teleconnections to Southern Ocean SST anomalies diagnosed from a surface mixed layer heat budget. *Geophys. Res. Lett.*, **38**.

Ciasto, L. M. and D. W. J. Thompson, 2008: Observations of large-scale ocean atmosphere interaction in the southern hemisphere. *J. Clim.*, **21**, 1244–1259, doi:10.1175/2007JCLI1809.1.

Collins, W. D., et al., 2006: The Community Climate System Model Version 3 (CCSM3). *J. Clim.*, **19**, 2122–2143, doi:10.1175/JCLI3761.1.

Dee, D. P., S. M. Uppala, and co authors, 2011: The ERA-Interim reanalysis: configuration and performance of the data assimilation system. *Quart. J. of the Royal Meteo. Soc.*, **137**, 553–597, doi:10.1002/qj.828.

Deser, C., M. A. Alexander, S.-P. Xie, and A. S. Phillips, 2010: Sea Surface Temperature Variability: Patterns and Mechanisms. *Annual Review of Marine Science*, **2**, 115–143, doi:10.1146/annurev-marine-120408-151453.

Deser, C., A. Capotondi, R. Saravanan, and A. S. Phillips, 2006: Tropical Pacific and Atlantic Climate Variability in CCSM3. *J. Clim.*, **19**, 2451, doi:10.1175/JCLI3759.1.

Ding, H., N. S. Keenlyside, and M. Latif, 2012: Impact of the Equatorial Atlantic on the El Niño Southern Oscillation. *Clim. Dyn.*, **38**, 1965–1972, doi:10.1007/s00382-011-1097-y.

Ding, Q., E. J. Steig, D. S. Battisti, and M. Küttel, 2011: Winter warming in West Antarctica caused by central tropical Pacific warming. *Nature Geoscience*, **4**, 398–403, doi:10.1038/ngeo1129.

Dréevillon, M., C. Cassou, and L. Terray, 2003: Model study of the North Atlantic region atmospheric response to autumn tropical Atlantic sea-surface-temperature anomalies. *Quart. J. Roy. Met. Soc.*, **129**, 2591–2611, doi:10.1256/qj.02.17.

Garreaud, R. D. and D. S. Battisti, 1999: Interannual (enso) and interdecadal (enso-like) variability in the southern hemisphere tropospheric circulation. *J. Clim.*, **12**, 2113–2123, doi:10.1175/1520-0442(1999)012⟨2113:IEAIEL⟩2.0.CO;2.

Haarsma, R. J. and W. Hazeleger, 2007: Extratropical Atmospheric Response to Equatorial Atlantic Cold Tongue Anomalies. *J. Clim.*, **20**, 2076–2091, doi:10.1175/JCLI4130.1.

Hodson, D. L. R., R. T. Sutton, C. Cassou, N. Keenlyside, Y. Okumura, and T. Zhou, 2010: Climate impacts of recent multidecadal changes in Atlantic Ocean Sea Surface Temperature: a multimodel comparison. *Clim. Dyn.*, **34**, 1041–1058, doi:10.1007/s00382-009-0571-2.

Hoskins, B. J. and T. Ambrizzi, 1993: Rossby Wave Propagation on a Realistic Longitudinally Varying Flow. *J. Atmos. Sci.*, **50**, 1661–1671, doi:10.1175/1520-0469(1993)050⟨1661:RWPOAR⟩2.0.CO;2.

Hurrell, J. W., J. J. Hack, A. S. Phillips, J. Caron, and J. Yin, 2006: The Dynamical Simulation of the Community Atmosphere Model Version 3 (CAM3). *J. Clim.*, **19**, 2162–2183, doi:10.1175/JCLI3762.1.

Jin, D. and B. P. Kirtman, 2009: Why the southern hemisphere enso responses lead enso. *J. Geophys. Res.*, **114**, D23 101, doi:10.1029/2009JD012657.

Karoly, D. J., 1989: Southern hemisphere circulation features associated with el niño-southern oscillation events. *J. Clim.*, **2**, 1239–1252, doi:10.1175/1520-0442(1989)002⟨1239:SHCFAW⟩2.0.CO;2.

Keenlyside, N. S. and M. Latif, 2007: Understanding Equatorial Atlantic Interannual Variability. *J. Clim.*, **20**, 131, doi:10.1175/JCLI3992.1.

Kushnir, Y., R. Seager, M. Ting, N. Naik, and J. Nakamura, 2010: Mechanisms of Tropical Atlantic SST Influence on North American Precipitation Variability. *J. Clim.*, **23**, 5610–5628, doi:10.1175/2010JCLI3172.1.

Lee, S.-K., C. Wang, and B. E. Mapes, 2009: A Simple Atmospheric Model of the Local and Teleconnection Responses to Tropical Heating Anomalies. *J. Clim.*, **22**, 272, doi:10.1175/2008JCLI2303.1.

Li, X., D. M. Holland, E. P. Gerber, and C. Yoo, 2014: Impacts of the north and tropical Atlantic Ocean on the Antarctic Peninsula and sea ice. *Nature*, **505**, 538–542, doi:10.1038/nature12945.

Luffman, J. J., A. S. Taschetto, and M. H. England, 2010: Global and Regional Climate Response to Late Twentieth-Century Warming over the Indian Ocean. *J. Clim.*, **23**, 1660–1674, doi:10.1175/2009JCLI3086.1.

Luo, J.-J., W. Sasaki, and Y. Masumoto, 2012: Indian Ocean warming modulates Pacific climate change. *PNAS*, **109**, 18 701–18 706, doi:10.1073/pnas.1210239109.

Marshall, G. J., 2007: Half-century seasonal relationships between the Southern Annular mode and Antarctic temperatures. *Int. J. Climatol.*, **27**, 373–383, doi:10.1002/joc.1407.

Marshall, G. J., A. Orr, N. P. M. van Lipzig, and J. C. King, 2006: The Impact of a Changing Southern Hemisphere Annular Mode on Antarctic Peninsula Summer Temperatures. *J. Clim.*, **19**, 5388, doi:10.1175/JCLI3844.1.

Mo, K. C. and R. W. Higgins, 1998: The pacific south american modes and tropical convection during the southern hemisphere winter. *Mon. Wea. Rev.*, **126**, 1581–1596, doi:10.1175/1520-0493(1998)126⟨1581:TPSAMA⟩2.0.CO;2.

Monaghan, A. J., D. H. Bromwich, W. Chapman, and J. C. Comiso, 2008: *J. Geophys. Res.*, **113**, D04 105, doi:10.1029/2007JD009094.

Okumura, Y. M., D. Schneider, C. Deser, and R. Wilson, 2012: Decadal-Interdecadal Climate Variability over Antarctica and Linkages to the Tropics: Analysis of Ice Core, Instrumental, and Tropical Proxy Data. *J. Clim.*, **25**, 7421–7441, doi:10.1175/JCLI-D-12-00050.1.

Parkinson, C. L. and D. J. Cavalieri, 2012: Antarctic sea ice variability and trends, 1979-2010. *The Cryosphere*, **6**, 871–880, doi:10.5194/tc-6-871-2012.

Raphael, M. N. and M. M. Holland, 2006: Twentieth century simulation of the southern hemisphere climate in coupled models. Part 1: large scale circulation variability. *Clim. Dyn.*, **26**, 217–228, doi:10.1007/s00382-005-0082-8.

Rasmusson, E. M. and K. Mo, 1993: Linkages between 200-mb Tropical and Extratropical Circulation Anomalies during the 1986-1989 ENSO Cycle. *J. Clim.*, **6**, 595–616, doi:10.1175/1520-0442(1993)006⟨0595:LBMTAE⟩2.0.CO;2.

Rayner, N. A., D. E. Parker, E. B. Horton, C. K. Folland, L. V. Alexander, D. P. Rowell, E. C. Kent, and A. Kaplan, 2003: Global analyses of sea surface temperature, sea ice, and night marine air temperature since the late nineteenth century. *J. Geophys. Res.*, **108**, 4407, doi:10.1029/2002JD002670.

Rignot, E., I. Velicogna, M. R. van den Broeke, A. Monaghan, and J. Lenaerts, 2011: Acceleration of the contribution of the greenland and antarctic ice sheets to sea level rise. *Geophys. Res. Lett.*, **38**, 5503, doi:10.1175.

Santoso, A., M. H. England, and W. Cai, 2012: Impact of Indo-Pacific Feedback Interactions on ENSO Dynamics Diagnosed Using Ensemble Climate Simulations. *J. Clim.*, **25**, 7743–7763, doi:10.1175/JCLI-D-11-00287.1.

Sardeshmukh, P. D. and B. J. Hoskins, 1988: The Generation of Global Rotational Flow by Steady Idealized Tropical Divergence. *J. Atmos. Sci.*, **45**, 1228–1251, doi:10.1175/1520-0469(1988)045⟨1228:TGOGRF⟩2.0.CO;2.

Schneider, D. P., C. Deser, and Y. Okumura, 2012a: An assessment and interpretation of the observed warming of West Antarctica in the austral spring. *Clim. Dyn.*, **38**, 323–347, doi:10.1007/s00382-010-0985-x.

Schneider, D. P., Y. Okumura, and C. Deser, 2012b: Observed Antarctic Interannual Climate Variability and Tropical Linkages. *J. Clim.*, **25**, 4048–4066, doi:10.1175/JCLI-D-11-00273.1.

Simpkins, G. R., L. M. Ciasto, and M. H. England, 2013: Observed variations in multidecadal Antarctic sea ice trends during 1979-2012. *Geophys. Res. Lett.*, **40**, 3643–3648, doi:10.1002/grl.50715.

Simpkins, G. R., L. M. Ciasto, D. W. J. Thompson, and M. H. England, 2012: Seasonal Relationships between Large-Scale Climate Variability and Antarctic Sea Ice Concentration. *J. Clim.*, **25**, 5451–5469, doi:10.1175/JCLI-D-11-00367.1.

Simpkins, G. R. and A. Y. Karpechko, 2012: Sensitivity of the southern annular mode to greenhouse gas emission scenarios. *Clim. Dyn.*, **38**, 563–572, doi:10.1007/s00382-011-1121-2.

Stammerjohn, S., R. Massom, D. Rind, and D. Martinson, 2012: Regions of rapid sea ice change: An inter-hemispheric seasonal comparison. *Geophys. Res. Lett.*, **39**, L06 501, doi:10.1029/2012GL050874.

Steig, E. J., Q. Ding, D. S. Battisti, and A. Jenkins, 2013: Recent climate and ice-sheet changes in West Antarctica compared with the past 2,000 years. *Nature*, **53**, 19–28, doi:10.1038/NGEO1778.

Steig, E. J., D. P. Schneider, S. D. Rutherford, M. E. Mann, J. C. Comiso, and D. T. Shindell, 2009: Warming of the Antarctic ice-sheet surface since the 1957 International Geophysical Year. *Nature*, **457**, 459–462, doi:10.1038/nature07669.

Taschetto, A. S. and T. Ambrizzi, 2012: Can Indian Ocean SST anomalies influence South American rainfall? *Clim. Dyn.*, **38**, 1615–1628, doi:10.1007/s00382-011-1165-3.

Taschetto, A. S., A. Sen Gupta, H. H. Hendon, C. C. Ummenhofer, and M. H. England, 2011: The Contribution of Indian Ocean Sea Surface Temperature Anomalies on Australian Summer Rainfall during El Niño Events. *J. Clim.*, **24**, 3734–3747, doi:10.1175/2011JCLI3885.1.

Thompson, D. W. J. and S. Solomon, 2002: Interpretation of recent southern hemisphere climate change. *Science*, **296**, 895–899, doi:10.1126/science.1069270.

Thompson, D. W. J., S. Solomon, P. J. Kushner, M. H. England, K. M. Grise, and D. J. Karoly, 2011: Signatures of the Antarctic ozone hole in Southern Hemisphere surface climate change. *Nature Geoscience*, **4**, 741–749, doi:10.1038/ngeo1296.

Timmermann, A., et al., 2010: Towards a quantitative understanding of millennial-scale Antarctic warming events. *Quat. Sci. Rev.*, **29**, 74–85, doi:10.1016/j.quascirev.2009.06.021.

Turner, J., et al., 2004: The SCAR READER Project: Toward a High-Quality Database of Mean Antarctic Meteorological Observations. *J. Clim.*, **17**, 2890–2898, doi:10.1175/1520-0442(2004)017⟨2890:TSRPTA⟩2.0.CO;2.

Turner, J., et al., 2005: Antarctic climate change during the last 50 years. *Int. J. Climatol.*, **25**, 279–294, doi:10.1002/joc.1130.

Tyrrell, G. C., D. J. Karoly, and J. L. McBride, 1996: Links between Tropical Convection and Variations of the Extratropical Circulation during TOGA COARE. *J. Atmos. Sci.*, **53**, 2735–2748, doi:10.1175/1520-0469(1996)053⟨2735:LBTCAV⟩2.0.CO;2.

Wang, C., 2006: An overlooked feature of tropical climate: Inter-Pacific-Atlantic variability. *Geophys. Res. Lett*, **33**, L12 702, doi:10.1029/2006GL026324.

List of Figures

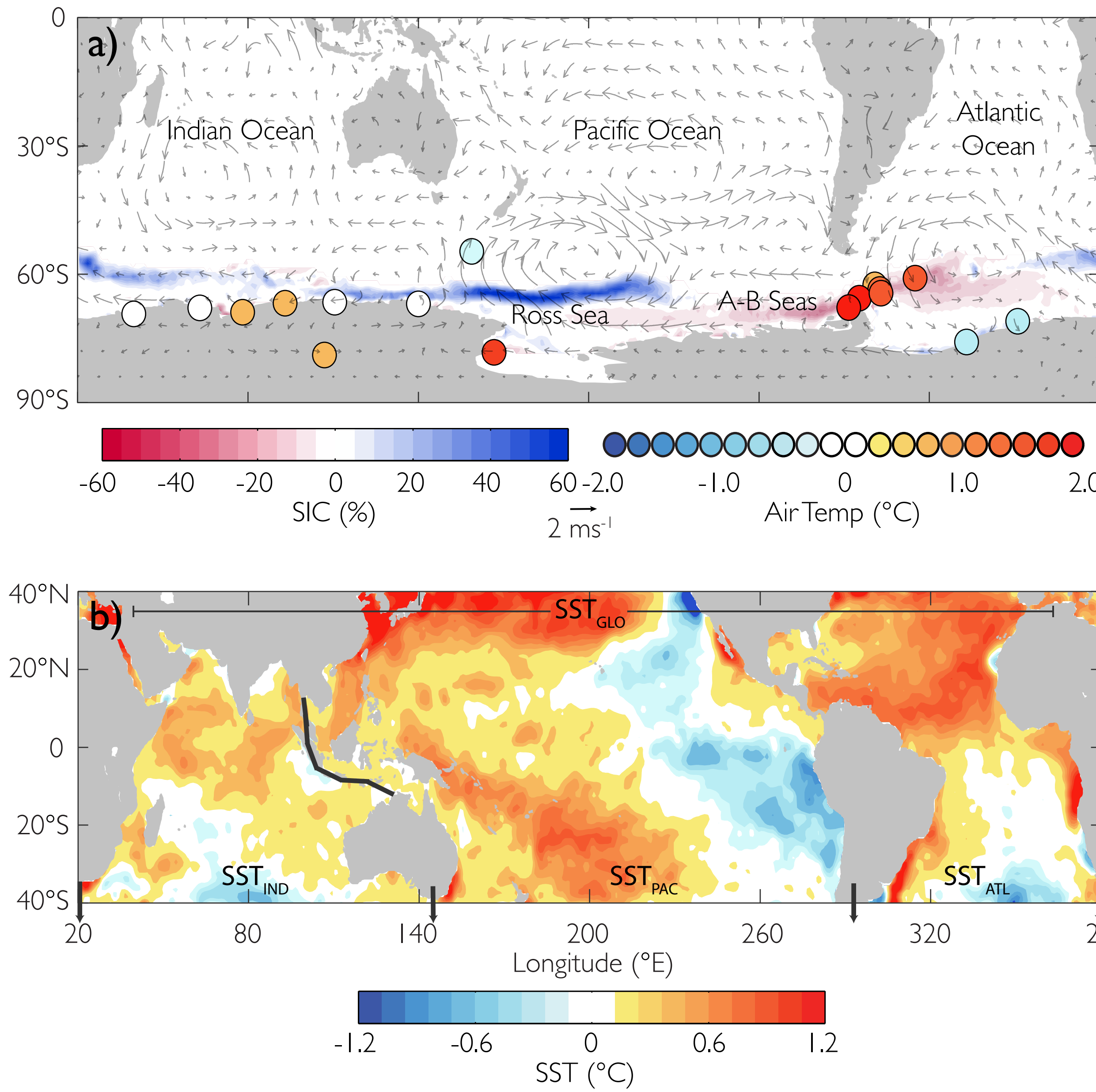

FIG. 1. Spring-time (September-November) trends in a) ERA-Interim 950-hPa wind (vectors), HadISST sea ice concentration (shading), and Antarctic station surface air temperature (colored dots), and b) HadISST sea surface temperature, all calculated over 1979-2009. Black lines in b) delineate the approximate ocean boundaries used for subsequent model experiments (SST$_{IND}$, SST$_{PAC}$, SST$_{ATL}$, and SST$_{GLO}$ - see Methods), with arrows signifying a straight southward extension to the Antarctic continent. A-B Seas in a) refers to the Amundsen-Bellingshausen Seas.

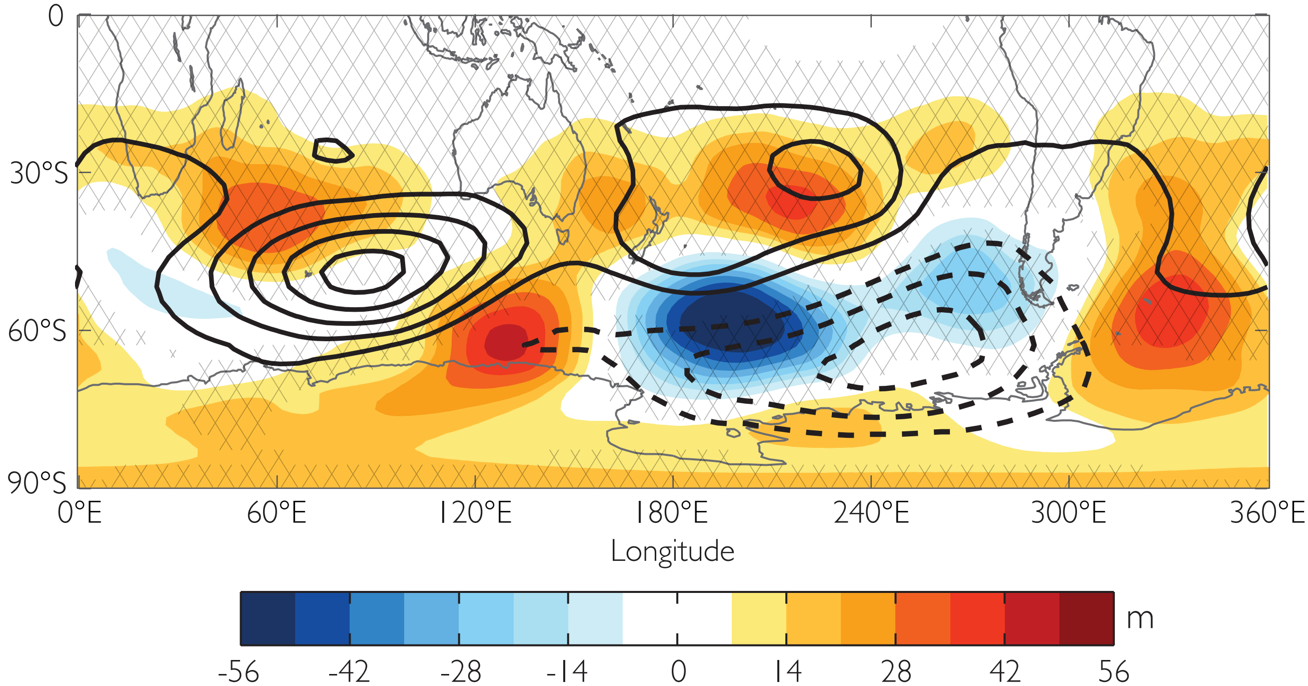

Fig. 2. Spring-time (September-November) Z_{500} trends from ERA-Interim (shading) and the SST_{GLO} model simulations (contours) calculated over 1979-2009. Solid (dashed) contours denote positive (negative) trends, and are drawn at intervals of 7m. Hatching indicates where ERA-Interim and SST_{GLO} agree on the sign of the trend.

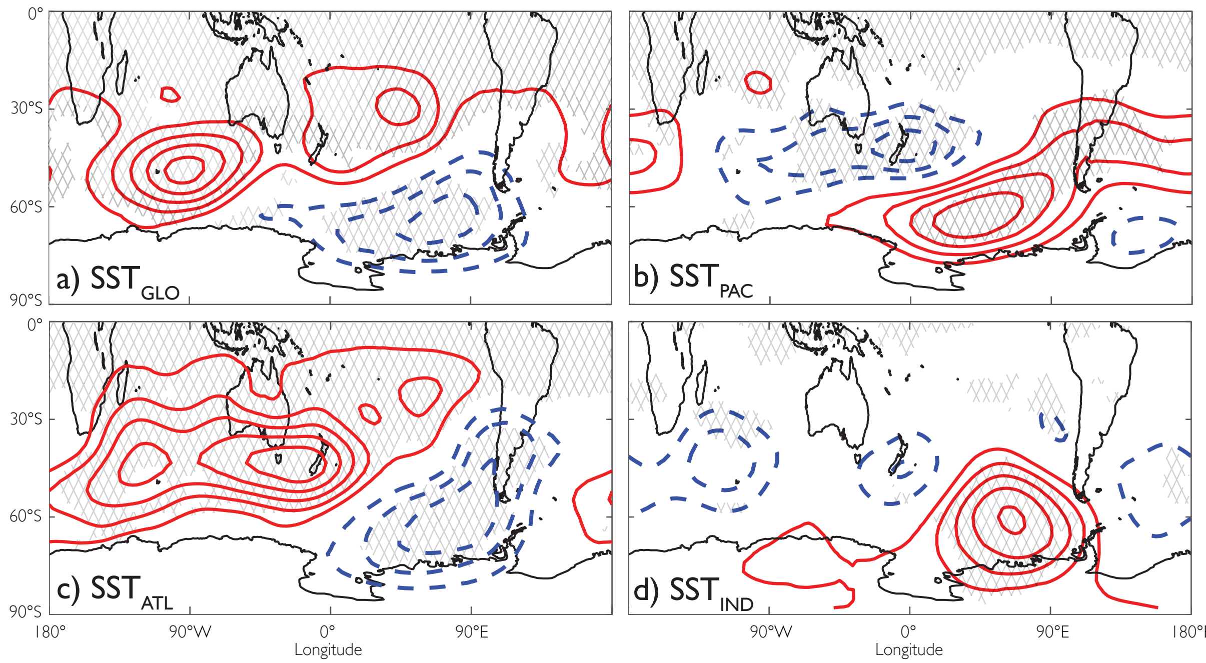

Fig. 3. Spring-time (September-November) Z_{500} trends for the various SST-forced atmospheric model experiments calculated over 1979-2009 (see text for explanation of forcing). Positive (negative) trends are denoted by solid-red (dashed-blue) contours, and are drawn at intervals of 7m; the zero-contour has been omitted. Hatching indicates where 9 of 12 ensemble members agree on the sign of the trend.

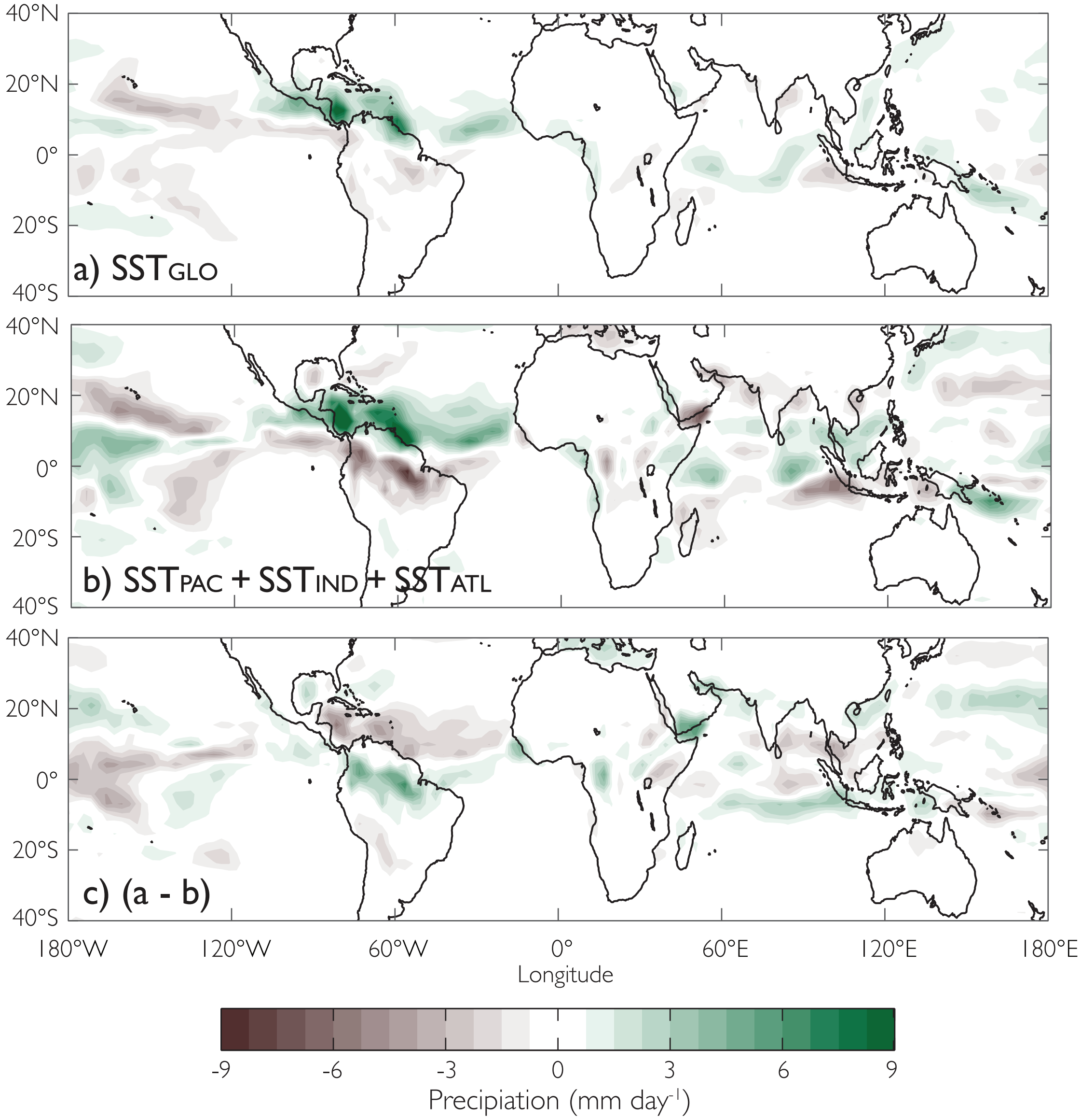

FIG. 4. Spring-time (September-November) convective precipitation trends from a) SST_{GLO}, b) the sum of SST_{PAC}, SST_{IND} and SST_{ATL}, and c) the difference between a) and b).

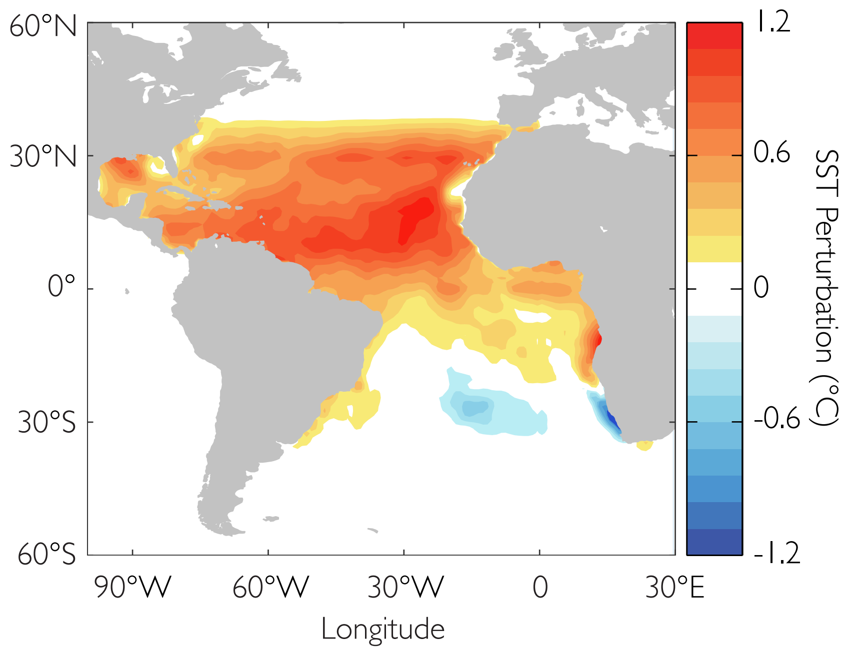

FIG. 5. Sea surface temperature perturbation used for the ATL$_{PERT}$ experiments (see text for details). Shading corresponds to the total spring-time (September-November) SST trends observed in the tropical Atlantic over 1979-2009, with tapering at latitudes >30°N/S.

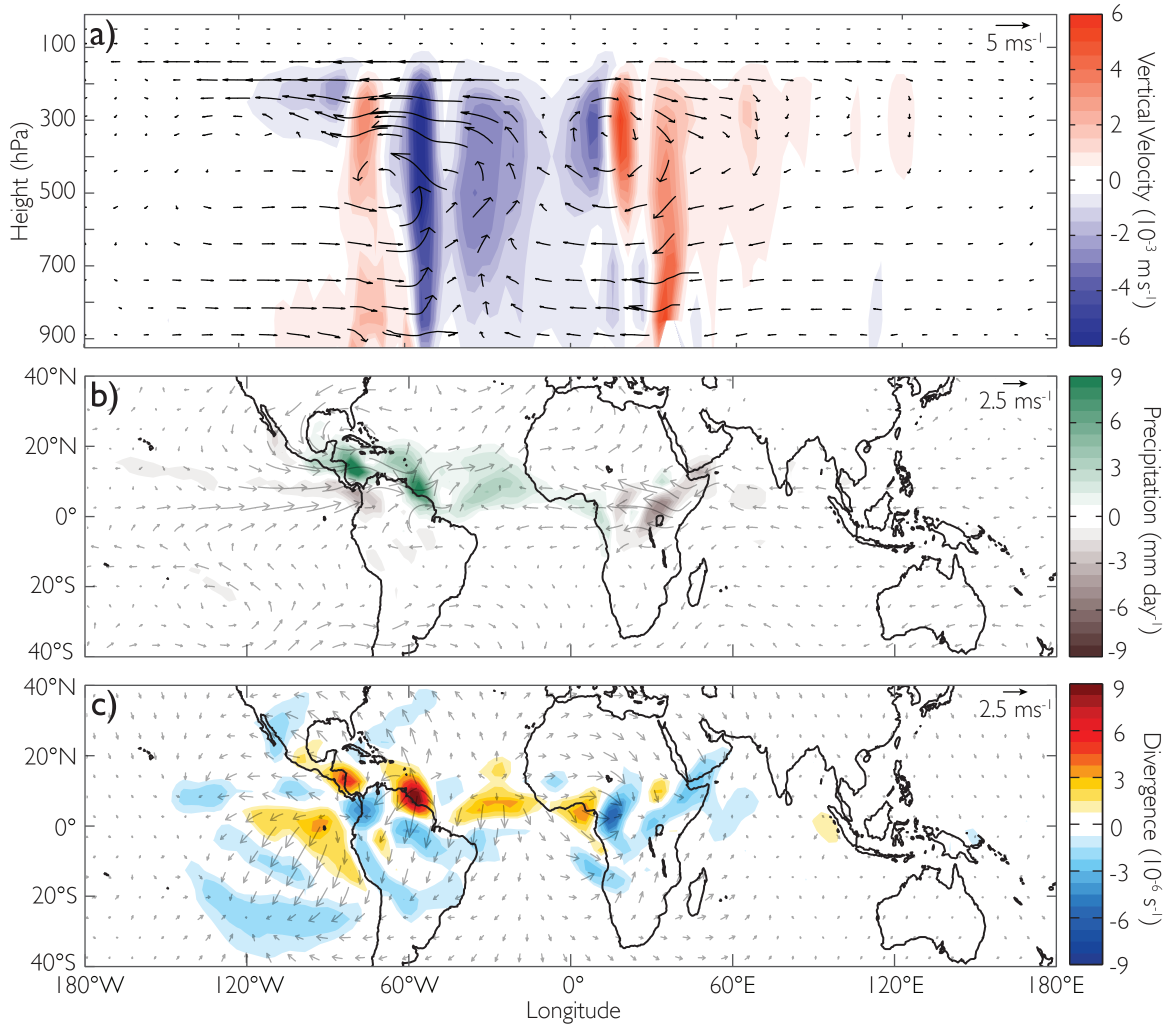

FIG. 6. 60-day average a) vertical velocity (shading) and U/W wind (vectors) anomalies averaged over 5°N-5°S, b) convective precipitation (shading) and 950-hPa wind (vectors), and c) 200-hPa divergence (shading) and divergent wind (vectors) anomalies from the ATL_{PERT} experiments. In panel a) red (blue) shading denotes downward (upward) flow, and to accentuate vertical motion, W vector anomalies have been scaled by a factor of 300.

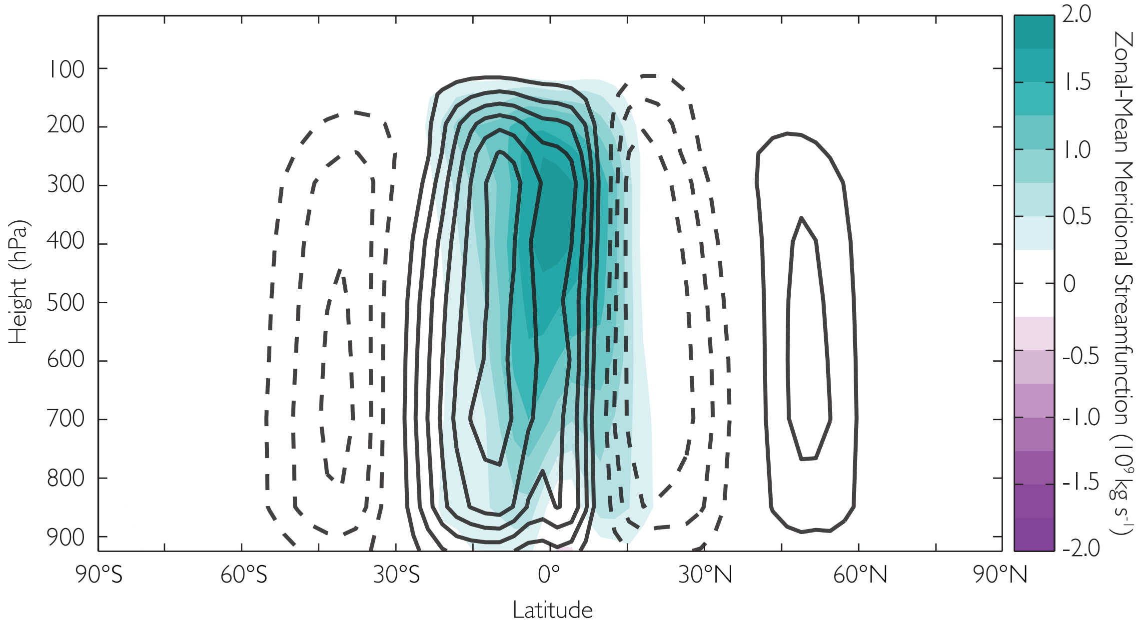

FIG. 7. 60-day average zonal-mean (180˚W - 180˚E) meridional streamfunction anomalies from the ATL$_{PERT}$ experiments (shading). Contours denote the climatological streamfunctions from the daily control simulations, and are drawn at intervals of 2 x 10^{10} kg s^{-1}. Solid (dashed) contours denote anti-clockwise (clockwise) flow.

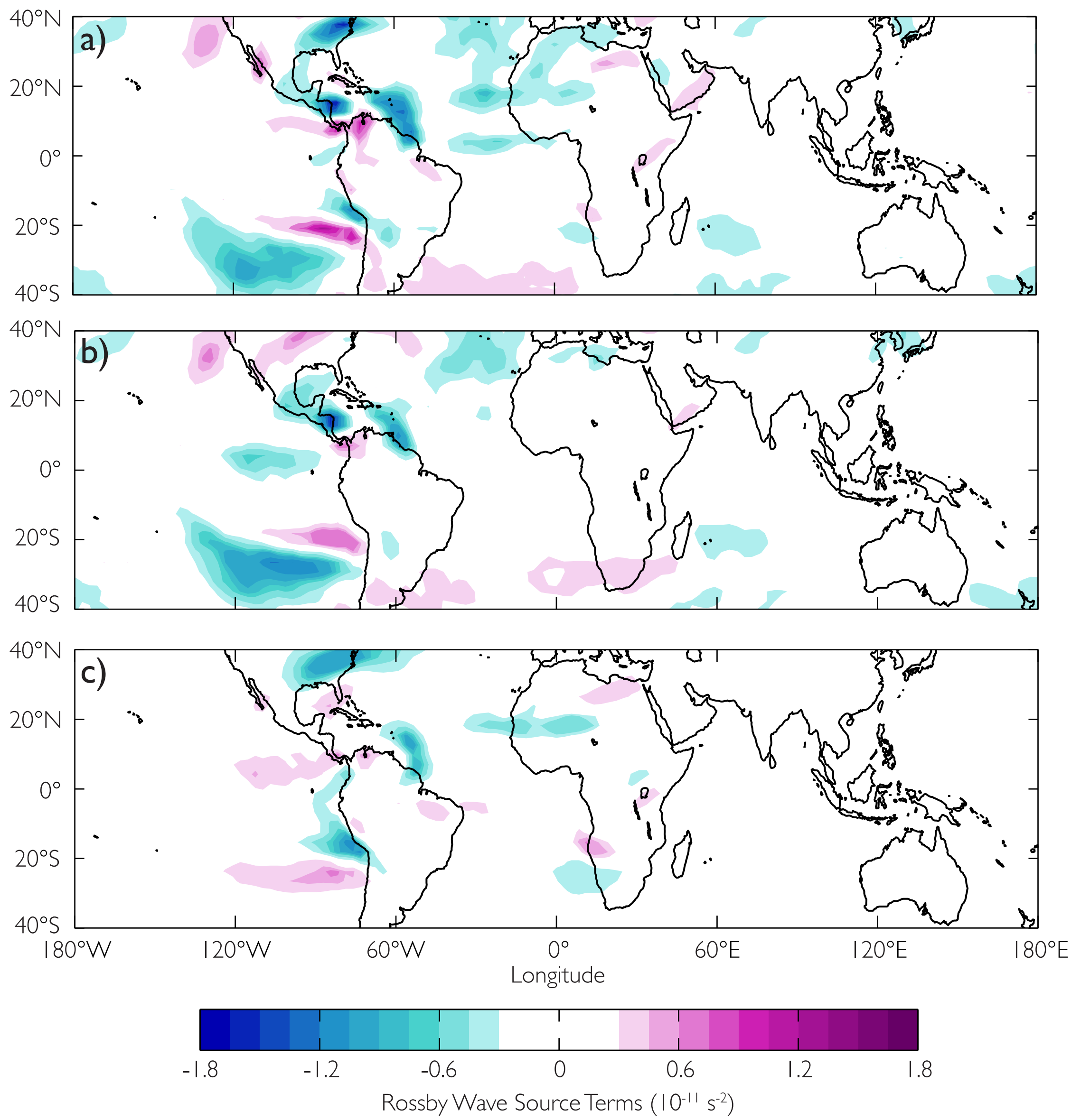

FIG. 8. 60-day average a) Rossby Wave Source, b) vortex stretching, and c) vorticity advection anomalies at 200-hPa from the ATL$_{PERT}$ experiments. See text for details of terms.

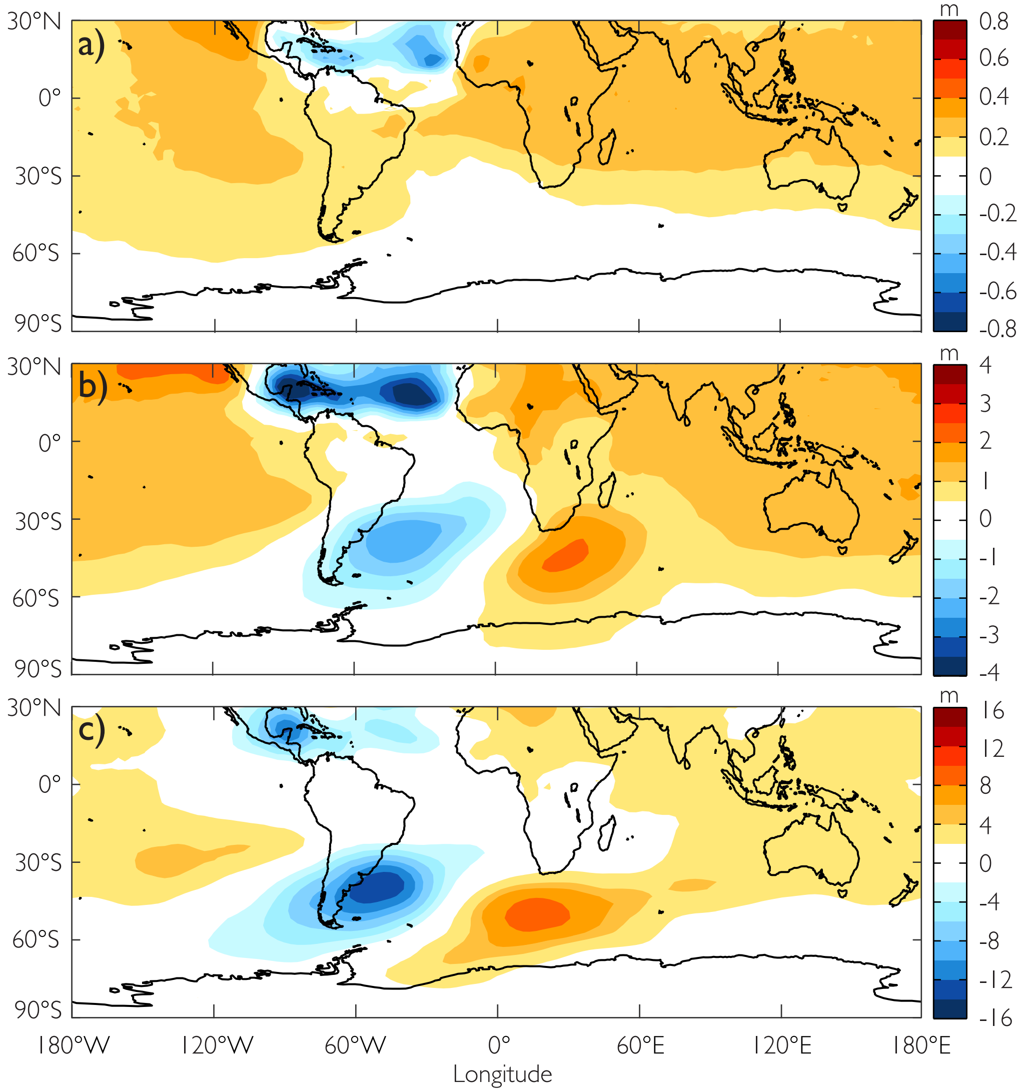

FIG. 9. Z_{500} anomalies from the ATL_{PERT} experiments averaged over days a) 1-3, b) 4-6, and c) 7-12. Note the contrasting color scales.

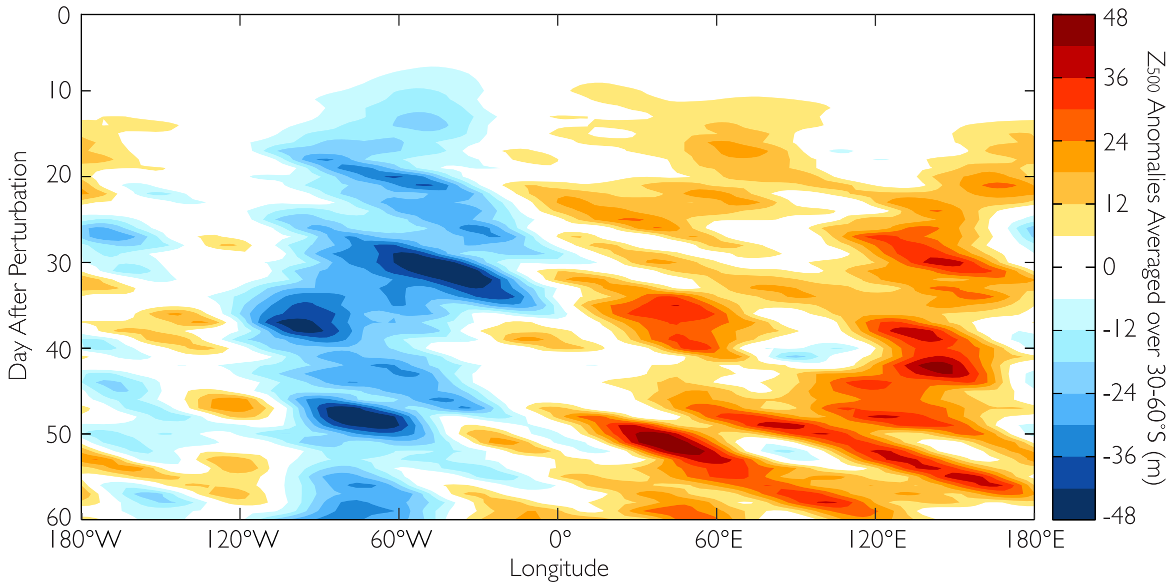

FIG. 10. Time-longitude Hovmöller of Z_{500} anomalies averaged over 30-60°S from the ATL_{PERT} experiments.

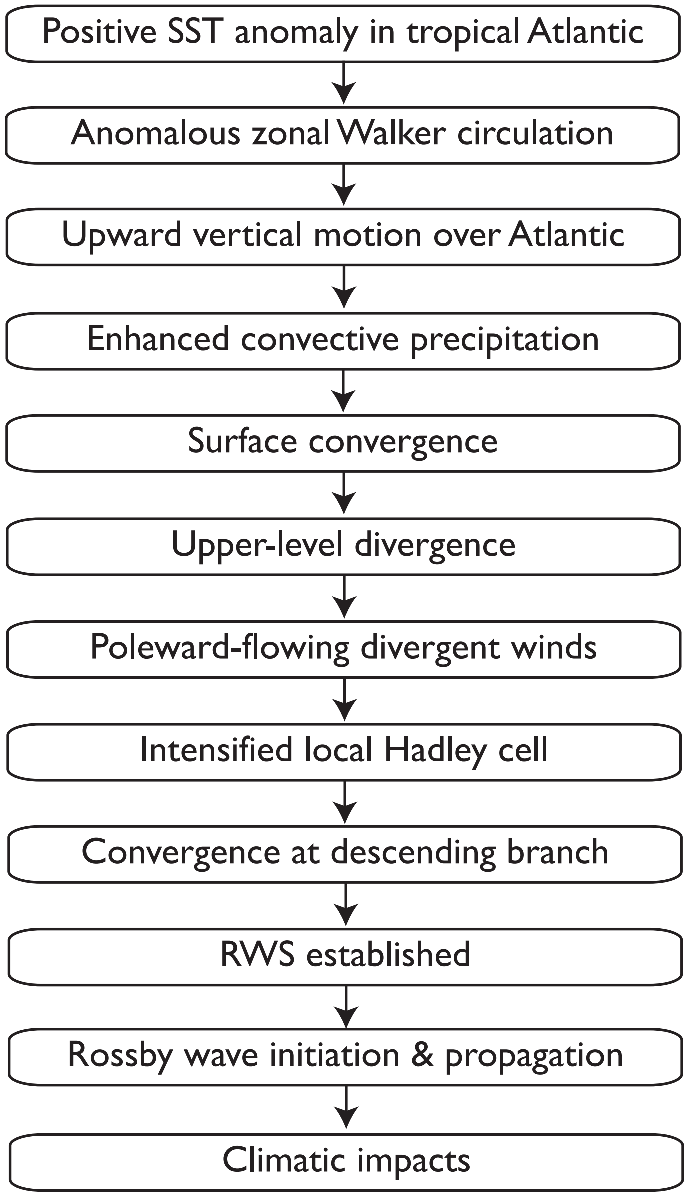

FIG. 11. Schematic diagram outlining how tropical Atlantic SST variability teleconnects to the Southern Hemisphere extratropics.

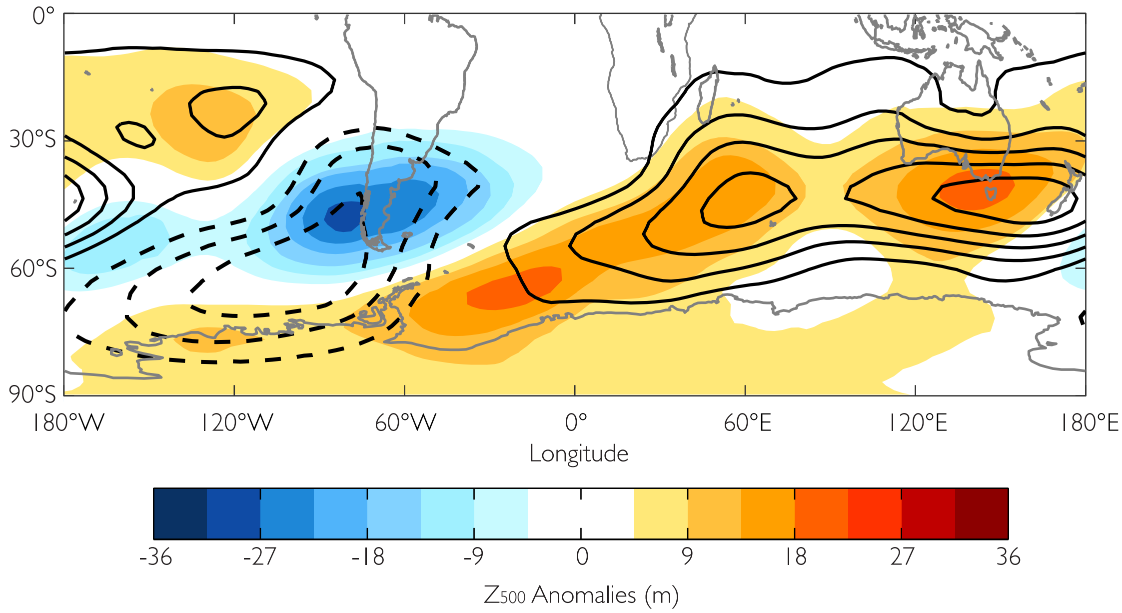

FIG. 12. 60-day average Z_{500} anomalies from the ATL_{PERT} experiments (shading), and spring-time (September-November) Z_{500} trends from the SST_{ATL} experiments calculated over 1979-2009 (contours). Solid (dashed) contours denote positive (negative) trends, and are drawn at intervals of 7m; the zero-contour has been omitted.

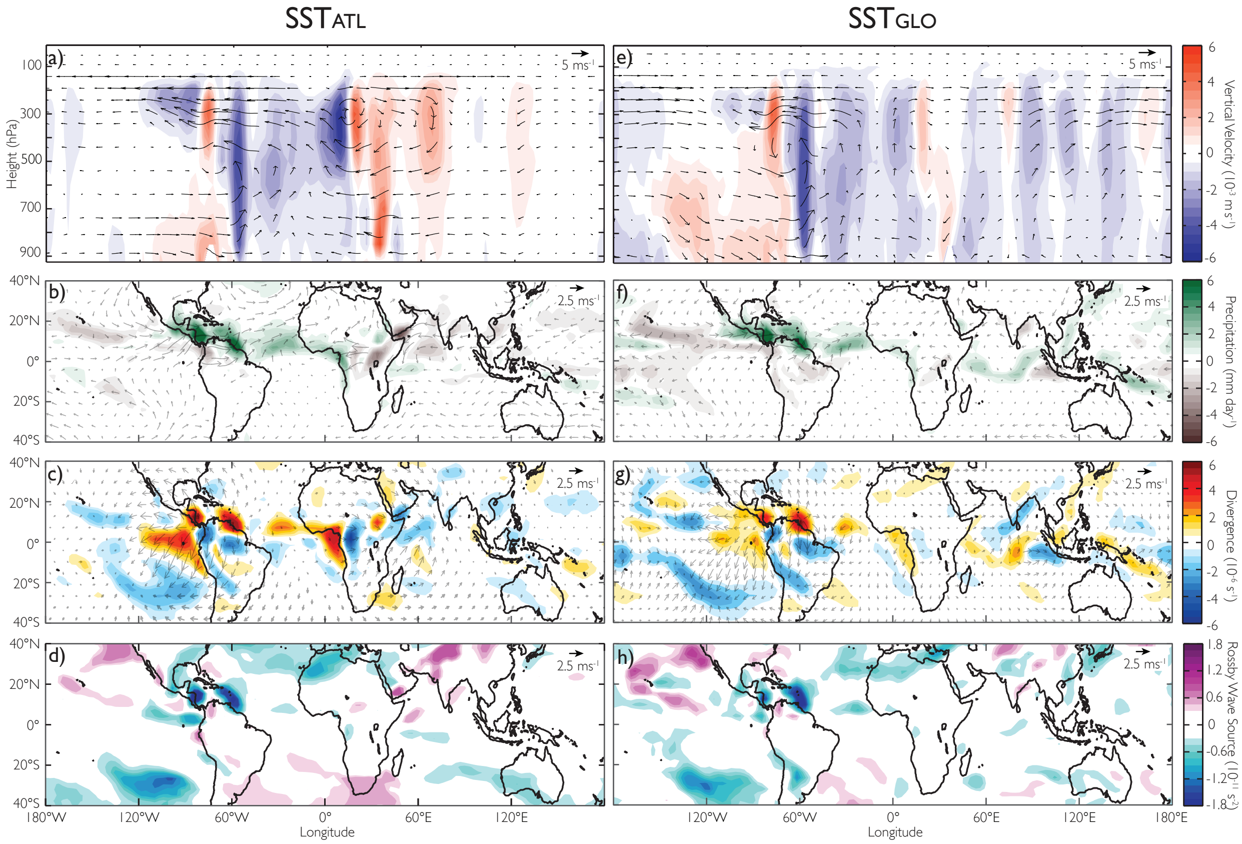

FIG. 13. Spring-time (September-November) trends in a) vertical velocity (shading) and U/W wind (vectors) averaged over 5°N-5°S, b) convective precipitation (shading) and 950-hPa wind (vectors), c) 200-hPa divergence (shading) and divergent wind (vectors), and d) Rossby Wave Source from the SST_{ATL} experiments, all calculated over 1979-2009. The right hand panels (e-h) show the equivalent trends from the SST_{GLO} experiments.

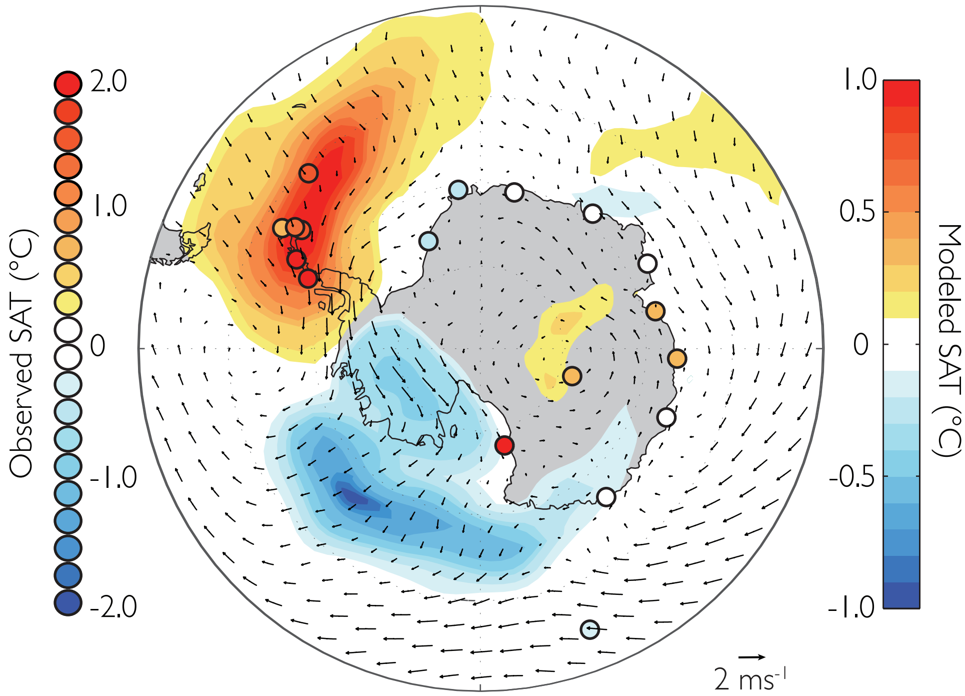

FIG. 14. Spring-time (September-November) trends in Antarctic station surface air temperature (colored dots), and modeled surface wind (vectors) and air temperature (shading) from the SST$_{ATL}$ experiments, all calculated over 1979-2009. Note the contrasting color axes for the observed and modeled temperature trends.